Environmental Research 213 (2022) 113614

Contents lists available at ScienceDirect

Environmental Research

journal homepage: www.elsevier.com/locate/envres

A green method for removing chromium (VI) from aqueous systems using novel silicon nanoparticles: Adsorption and interaction mechanisms

Sajid Mehmood [a,b,1], Mohsin Mahmood [a,b,1], Avelino Núñez-Delgado [c], Juha M. Alatalo [d], Ahmed S. Elrys [e], Muhammad Rizwan [f], Jiechang Weng [g], Weidong Li [a,b,*], Waqas Ahmed [a,b,**]

[a] Key Laboratory of Agro-Forestry Environmental Processes and Ecological Regulation of Hainan Province, Hainan University, Haikou, 570100, China
[b] College of Ecology and Environment, Hainan University, Haikou City, 570100, China
[c] Department of Soil Science and Agricultural Chemistry, Engineering Polytechnic School, University of Santiago de Compostela, Campus Univ. s/n, 27002, Lugo, Univ. Santiago de Compostela, Spain
[d] Environmental Science Center, Qatar University, Doha, Qatar
[e] Soil Science Department, Faculty of Agriculture, Zagazig University, Zagazig, 44511, Egypt
[f] Agricultural Research Station, Office of VP for Research & Graduate Studies, Qatar University, 2713, Doha, Qatar
[g] Hainan Provincial Ecological and Environmental Monitoring Center, 571126, China

ARTICLE INFO

Keywords:
Silicon nanoparticles
Horsetail (*Equisetum arvense*)
Green synthesis
Chromium
Adsorption

ABSTRACT

In the present study, we used the horsetail plant (*Equisetum arvense*) as a green source to synthesize silicon nanoparticles (GS-SiNPs), considering that it could be an effective adsorbent for removing chromium (Cr (VI)) from aqueous solutions. The characterization of GS-SiNPs was performed via Brunauer-Emmett-Teller (BET), scanning electron microscopy (SEM), energy dispersive spectroscopy (EDS), transmission electron microscopy (TEM), X-ray diffraction (XRD), Fourier transform infrared spectroscopy (FTIR), and X-ray photo electron spectroscopy (XPS) techniques. The batch test results of Cr (VI) adsorption on GS-SiNPs showed a high adsorption capacity, reaching 87.9% of the amount added. The pseudo-second order kinetic model was able to comprehensively explain the adsorption kinetics and provided a maximum Cr (VI) adsorption capacity (Q_e) of 3.28 mg g^{-1} ($R^2 = 90.68$), indicating fast initial adsorption by the diffusion process. The Langmuir isotherm model fitted the experimental data, and accurately simulated the adsorption of Cr (VI) on GS-SiNPs ($R^2 = 97.79$). FTIR and XPS spectroscopy gave further confirmation that the main mechanism was ion exchange with Cr and surface complexation through –OH and –COOH. Overall, the results of the research can be of relevance as regards a green and new alternative for the removal of Cr (VI) pollution from affected environments.

1. Introduction

Novel and sustainable methodologies under the label 'Green nanotechnology' have been recently developed for nanoparticle synthesis, with the aim of improving water quality and reducing the exposure of humans and ecosystems to pollutants (Naikoo et al., 2021; Sharma et al., 2021). With industrialization, climate change, and the expansion of urban areas, pollution has become a global challenge which requires urgent attention (Irfan et al., 2021). Soil, water, and air pollution are the three major types of pollution. Among them, water pollution is the most common and is related to a variety of fatal diseases, which globally cause the death of about two million people annually (Chen et al., 2019). In recent years, China has experienced rapid industrialization and urbanization, resulting in serious water pollution episodes (Zhou et al., 2021). This is an alarming issue as it threatens the safety of the environment and food, which in turn influences human health. Consequently, China, which is inhabited by about 20% of the world's population, gives great importance to water pollution, being a priority in environmental safety measures (Chen et al., 2018).

On account of natural and anthropogenic sources, heavy metals

* Corresponding author. Key Laboratory of Agro-Forestry Environmental Processes and Ecological Regulation of Hainan Province, Hainan University, Haikou, 570100, China.
** Corresponding author. Key Laboratory of Agro-Forestry Environmental Processes and Ecological Regulation of Hainan Province, Hainan University, Haikou, 570100, China.
E-mail addresses: weidongli@hainanu.edu.cn (W. Li), drwaqas@hainanu.edu.cn (W. Ahmed).
[1] These authors contributed equally to this work.

https://doi.org/10.1016/j.envres.2022.113614
Received 5 February 2022; Received in revised form 24 May 2022; Accepted 2 June 2022
Available online 13 June 2022

(HMs) are the pollutants most frequently released into water bodies (Ajiboye et al., 2021; Azimi et al., 2017). Over the years, increases in the maximum permissible limit of HMs in drinking water have become a major public concern in most parts of the world (Egbueri, 2020; Egbueri et al., 2020; Muleya et al., 2020; Sholehhudin et al., 2021; Toure et al., 2019). Hexavalent chromium (Cr (VI)), as one of these HMs, is carcinogenic and toxic, and has become a major source of public health problems due to its non-biodegradable nature, high solubility in aqueous environments (Wani et al., 2018), and its use and improper handling in various industries (leather, tanning, textiles, and electroplating) (Lou et al., 2021). Considering the harmful effects of Cr (VI) on human health, the World Health Organization (WHO) (Codex Alimentarius Commission, 1997) and the Environmental Protection Agency have set the maximum concentration levels in drinking water at 50 and 100 μg L^{-1}, respectively (Dianyi Yu, 2010). Increasing daily intake of Cr (VI) (0.01–0.09 mg day^{-1}) can cause skin inflammation, liver and kidney damage, lung congestion, vomiting, and ulcers (Hu et al., 2007).

Green synthesized nanoparticles are considered to be a future trend in agriculture and forestry, on account of their unique physical and chemical properties and capacity to act as a productive catalyst in the oxidation reaction used to treat effluent water from industries (Ferrari, 2005; Saravanan et al., 2021). Specifically, silicon (Si) nanoparticles (SiNPs) have attracted tremendous attention in their application as remediators for HMs, owing to their high adsorption capacity (Bhat and Venkatram, 2019; Farajzadeh Memari-Tabrizi et al., 2021), and their great potential in improving agriculture yield (El-Saadony et al., 2021). Due to their chelating properties, SiNPs have high potential for water remediation (Iqbal et al., 2016; Yadav et al., 2021). Recently, the biosynthesis of SiNPs has proven to be more effective, economical, and valuable than chemical synthesis in the remediation of HMs, and thus in achieving sustainable development for the environment (Adinarayana et al., 2020; Roychoudhury, 2020; Shafiei et al., 2021).

As potential green source of Si, horsetail (*Equisetum arvense*) is a rush-like perennial related to ferns, with hollow, jointed stems containing large quantities of silica and silicic acids (Vivancos et al., 2016). In view of that, it could be explored as a low-cost and Si-rich source for the green synthesis of SiNPs, and for the removal of HMs by adsorption. Also favoring it, this plant has worldwide availability, proliferous growth, and ability to cover a stagnant surface within a short duration of time. To note that, up to date, previous studies were limited to the use of horsetail for the synthesis of SiNPs and did not study its role in Cr removal by adsorption (Annenkov et al., 2020; García-Gaytán et al., 2019).

Taking all that background into account, the idea of using green synthesized nanoparticles to treat Cr is not new (Jin et al., 2018; Mohan et al., 2015), however, there are many challenges which have yet to be overcome. For instance, nanoparticles, used for in situ remediation, are released to the environment to remove contaminants (Limbach et al., 2008). Upon the release of nanoparticles their mobility and effective surface area and present a toxicity hazard to the environment (Sorwat et al., 2020). The main challenge lies in maintaining the performance of nanoparticles towards Cr removal, while curtailing the potential disadvantages associated with their application. The main objective of this study was to bring about green synthesis of silicon nanoparticles using the rapid, eco-friendly and low-cost horsetail plant extract method to remove Cr (VI) from the aqueous environment. These green synthesized SiNPs were characterized by Brunauer-Emmett-Teller (BET), scanning electron microscopy (SEM), energy dispersive spectroscopy (EDS), transmission electron microscopy (TEM), X-ray diffraction (XRD), Fourier transform infrared spectroscopy (FTIR), and X-ray photo electron spectroscopy (XPS) techniques. The results of the research could be of relevance as regards a new and green alternative to remove a dangerous pollutant from environmental compartments.

2. Materials and methods

2.1. Materials, chemicals, and reagents

All chemicals and reagents used in this study were of analytical grade, provided by Fuchen Chemical Reagents, China. Horsetail plants for green synthesis of SiNPs were collected from Shaoguan City, China. Ultra-pure water (18.2 MΩ cm^{-1} resistivity; Milli-Q, Germany) was used throughout the experiment.

2.2. Preparation of plant extract

For the preparation of plant extract method of Sharma et al. (2021) with slight modification was adopted. Briefly, harvested horsetail plants were washed several times with ultrapure deionized water to remove dust particles and dried at room temperature (25 °C) for six days until the weight stabilized. Dried plants were ground in a Worbush grinder (Dongguan Huatai Electric Co., Ltd., China) for 4 min. Then 5 g of finely powdered horsetail plants were heated in 100 mL of deionized water at 55 °C for 45 min. After that, the heated leaves were filtered and used for green synthesis of SiNPs (GS-SiNPs).

2.3. Green synthesis of SiNPs

Horsetail plants were used as a green Si precursor. The synthesis of SiNPs was performed by following the protocols set out by Mohd et al. (2017) (Mohd et al., 2017), with slight modifications for the extraction of Si from horsetail plants. The prepared plant extract was refluxed with sodium hydroxide (NaOH; 1.0 N) for 1 h. The following reaction was rationalized after refluxion of plant extract with NaOH:

$$\boldsymbol{Si(Horsetail\ plant) + NaOH = Na_2SiO_3 + H_2O}$$

The SiNPs were separated from sodium silicate (Na_2SiO_3) by adding hydrochloric acid (HCl; 0.1 M) drop-wise until the pH of the solution reached 6.0 (Chapa-González et al., 2018). The addition of HCl to Na_2SiO_3 produced a NaCl and SiO_2 reaction which can be rationalized as:

$$\boldsymbol{Na_2SiO_3 + 2HCl = 2NaCl + SiO_2 + H_2O}$$

After that, washing with ethanol and water was performed multiple times to remove formed NaCl, and the resulting precipitate was collected by centrifugation for 10 min at 9000 G. The final product was then placed in an oven at 50 °C for 24 h. After drying, the GS-SiNPs were placed in a vial for characterization and further analysis.

2.4. Characterization of GS-SiNPs

A TriStar II 3020 Version 3.02 Serial # 2154 (Micromeritics Instrument Corporation, China) equipment was used to determine the pore size distribution and BET (Brunauer, Emmett and Teller) surface area of GS-SiNPs, under the following conditions: Analysis adsorptive: N_2, analysis bath temperature: −195.8 °C, equilibration interval: 5 s, and sample density: 1.00 g cm^{-3}. Micromorphological structures of GS-SiNPs were characterized by a Gemini 300 (Shanghai, China) thermal field emission scanning electron microscope with the energy spectrum of: Oxford X-MAX and Electron Backscatter Diffraction: Oxford SYMMETRYS, and by a transmission electron microscope (TEM) with instrument model FEI Talos F200X (USA), accelerating voltage 200 KV, camera length 520 mm, and electron wavelength 0.0251 Å. The iS10 FT-IR spectrometer from Nicolli (USA) (400-4000 cm^{-1}, resolution 4.00 cm^{-1}, scans 64 times) was used to detect the surface functional groups of GS-SiNPs. XRD wide-angle diffraction (D8 ADVANCE X-ray diffractometer from Bruker, Germany) was used to obtain crystallinity of GS-SiNPs. An X-ray photoelectron spectroscopy test (250Xi from Thermo Fisher Scientific, USA) was used to examine the composition and valence state of GS-SiNPs, while zeta potential was measured using a Nano Brook

Zeta PALS Potential Analyzer (Brookhaven Instruments, Holtsville, NY, USA).

2.5. Adsorptive removal procedure of Cr (VI) from water with GS-SiNPs

Batch studies of Cr (VI) adsorption were carried out in Erlenmeyer flasks at different pH values, contact time intervals, temperatures, adsorbent dose and initial Cr (VI) concentrations. In the adsorption experiment, the pH values of the solution varied between 2 and 7, the contact times between 0 and 160 min, adsorbent dose 10–130 mg L^{-1} and the Cr (VI) concentrations between 5 and 100 mg L^{-1}. For each test, a specific amount of the adsorbent was added to the reaction solution. The solution was then subjected to thermostatic magnetic stirring (using S10-3 equipment, Taizhou Zhejiang, China) for 12 h to reach equilibrium. Before adding the adsorbent, the pH of the solution was adjusted with 1 M NaOH/HNO_3. Within the specified sampling interval, a 5 mL aliquot of the solution was collected from each sample and filtered with a 0.45 μm syringe filter. The concentration of Cr (VI) present in the solution was finally measured using an ultraviolet–visible spectrophotometer (Thermo Fisher Scientific, USA). The adsorption capacity (Q_e) of the adsorbent was then calculated with the formula shown below.

While the calculation of percentage removal of Cr (VI) and the adsorption capacity of the adsorbent was done by equations (1) and (2), respectively:

$$Removal\ (\%) = \frac{(C_0 - C_e)}{C_0} \times 100 \tag{1}$$

$$Qe\ (mg/g) = \frac{(C_0 - C_e)}{m} \times V \tag{2}$$

where qe (mg/g) is the adsorption capacity, C_o (mg/L) is the initial metal ion concentration in solution, C_e (mg/L) is the metal ion concentration remaining in solution at equilibrium, V (litres) represents the volume of solution used for the adsorption and m (mg) is the mass of the adsorbent used.

Data corresponding to the adsorption isotherms were obtained and then modeled using the Langmuir (Eq. (3)) and Freundlich (Eq. (4)) equations (Ayawei et al., 2017), expressed as follows:

$$Q_e = \frac{Q_m K_L C_e}{1 + K_L C_e} \tag{3}$$

$$Q_e = Log\ K_F + \frac{1}{n} Log\ C_e \tag{4}$$

where Q_e (mg g^{-1}) is the adsorption capacity for the pollutant which is present in a specific concentration (C_e); Q_m is the maximum adsorption capacity for the contaminant; K_L (L mg^{-1}) and K_F (mg g^{-1}) are the constants of the Langmuir and Freundlich adsorption isotherms, respectively; and n is an empirical constant of Freundlich's related to the adsorption intensity, which fluctuates with the heterogeneity of the material.

Pseudo-first order, pseudo-second order, and intraparticle diffusion models were used to analyze the adsorption kinetics (Wang et al., 2016), which are often expressed in linear form as follows:

$$\mathrm{Ln}\left(1 - \frac{q_t}{q_e}\right) = -k_1 \times t \tag{5}$$

$$\frac{t}{q_t} = \frac{1}{k_2 q_e^2} + \frac{t}{q_e} \tag{6}$$

where k_1 (1/min) and k_2 (g $mmol^{-1}$ min^{-1}) are the kinetic constants.

2.6. Desorption and regeneration experiments

The reusability of GS-SiNPs in actual environments was investigated to check its regeneration potential. In the desorption experiment, hydrochloric acid (HCl) solutions with five different concentrations (0.1, 0.2, 0.5, 1.0 and 1.5 mol L^{-1}) were used as strip pants. Small amounts (100 mg) of GS-SiNPs after Cr (VI) adsorption were put into 50 mL HCl solutions and the mixtures kept being subjected to desorption for half an hour. The supernatant was sampled after filtration, and the Cr (VI) concentration was measured. The measuring procedures were the same as the ones for the adsorption experiments. In the regeneration experiment, after performing Cr (VI) desorption with 1.0 mol L^{-1} HCl, adsorbent was collected and washed with double-distilled water (DDW), following separation from the eluent by centrifugation. After that, it was washed with DDW 3 times. Finally, the adsorbent was dried at 80 °C for 12 h. The adsorbent was reused in subsequent adsorption experiments, and the process was repeated for five cycles.

2.7. Statistical analysis

The investigation into the adsorption of Cr (VI) on GS-SiNPs was performed in triplicates. Statistix 8.0 was used to perform statistical analysis of the data. Mean values of measurements with standard deviation were used in the diagrams, adsorption isotherms and adsorption kinetic models. A significance level of $p < 0.05$ was used throughout the study.

3. Results and discussion

3.1. Characterization of green synthesized silicon nanoparticles

The green synthesized silicon nanoparticles (GS-SiNPs) were characterized by SEM (Fig. 1), which shows that micrographs are compact and uneven, with uniform size. Fig. 2 shows elemental mapping images of the same sample, whereas the weight proportion of elements was calculated by EDS as 65.6%, 26.4%, and 8.0% for C, O, and Si, respectively. The distribution of elements confirms the presence of Si. The presence of O and C can enhance the adsorption capacity of GS-SiNPs towards water pollutants (Ahmed et al., 2021a; Philippou et al., 2019). The particle morphology was examined using TEM analysis. TEM images of GS-SiNPs clearly show the size, shape, and micro-structure of the adsorbent (Fig. 3). They revealed the presence of a layered, porous structure, with unique, bulky, multi-layered aggregations, monodispersed with uniform dispersion of NPs, and with a BJH adsorption average pore diameter (4V/A) of 15.01 nm. With the increased porous structure, GS-SiNPs provided a greater accessible area with maximum adsorption capacity, and their adoption into actual environments would have clear practical implications (Sharma et al., 2021).

Fig. 4 shows the N_2 adsorption-desorption isotherm, and the inset shows the pore size distribution of GS-SiNPs. The curve of GS-SiNPs was consistent with the type-IV isotherm and H3 hysteresis loop (Sing, 2007), showing the existence of mesopores. The desorption curve shows a hysteresis loop as it does not coincide with the adsorption curve, which is a clear indication of a strong interaction between sorbent and adsorbate (Ahmed et al., 2021b). The adsorption average pore diameter (4V/A by BET) of GS-SiNPs was recorded to be 10.261 nm, and the average nanoparticle particle size was 411.70 nm. Indeed, the higher surface area could be helpful in binding the heavy metals on the accessible active sites (Ahmed et al., 2021a; Huang et al., 2018). The BET surface area of GS-SiNPs, meanwhile, was recorded to be 14.57 m^2 g^{-1}. The single point adsorption total pore volume of pores was recorded to be less than 130.99 nm, and the diameter at P/Po was 0.038 cm^3 g^{-1}. The obtained values indicate that GS-SiNPs could be a promising adsorbent choice for the adsorption of pollutants from water (Sharma et al., 2021).

The XRD was accessed as described the procedure in Sect. 2.4 to know the product crystallinity, size and phases respectively. As received spectrum from XRD (Fig. 5A), exhibited very well-defined peaks related to the available data of powder sample and matched with the JCPDS

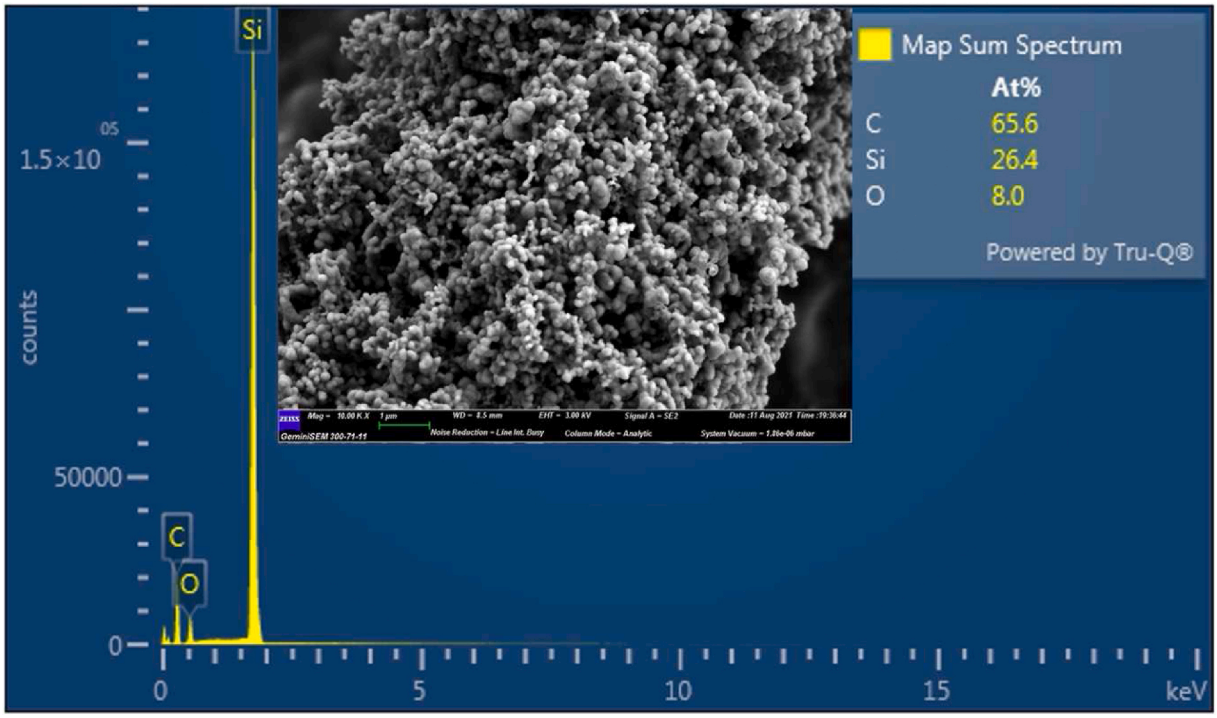

Fig. 1. SEM-EDX images of green synthesized silicon nanoparticles (GS-SiNPs). (For interpretation of the references to colour in this figure legend, the reader is referred to the Web version of this article.)

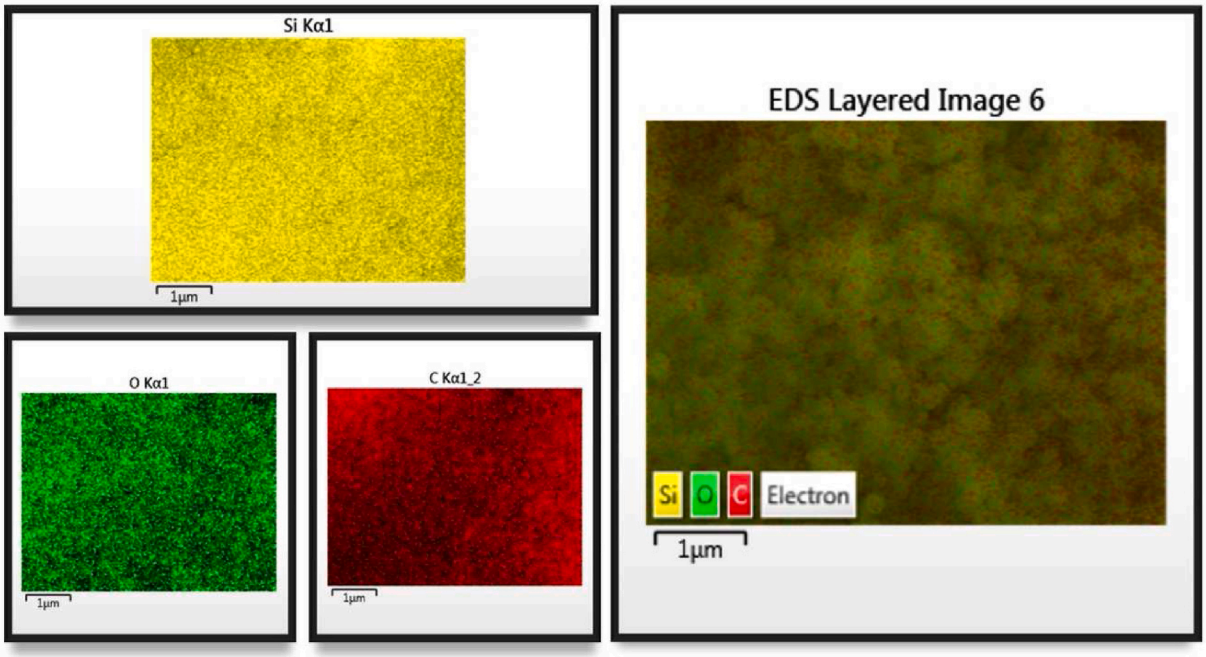

Fig. 2. Elemental mappings of the homogenous dispersion of silicon (Si), oxygen (O), and carbon (C) elements in green synthesized silicon nanoparticles (GS-SiNPs). (For interpretation of the references to colour in this figure legend, the reader is referred to the Web version of this article.)

card No. 39–1346. The peaks positions are as 28.40 <111>, 47.20 <220>, 56.05 <311>, 69.10 <400> and 76.30 <331> are clearly indexed with silicon phase (Si-NPs) (Wahab et al., 2020). The sharpening of the peaks clearly indicates that the particles are in the regime of nanoparticles (Adinarayana et al., 2020; Jose et al., 2016; Zaumseil, 2015). There are no other peaks related to any impurities had been observed in the spectrum, which states that the processed material is highly pure and well crystalline in nature (Gupta and Wiggers, 2011; Wahab et al., 2020).

Moreover, the surface functional groups of GS-SiNPs were further analyzed by FTIR before and after adsorption of Cr (VI). The FTIR spectra were recorded by drop-casting the GS-SiNPs sample onto KBr pellets (Fig. 5B). These data reveal major Si–O–Si symmetric bond stretching, at 474 cm^{-1}, while the peak at 1069 cm^{-1} is due to the asymmetric stretching of the Si–O–Si bond. These peaks are considered the characteristic peaks of SiNPs (Sharma et al., 2021). The bands at

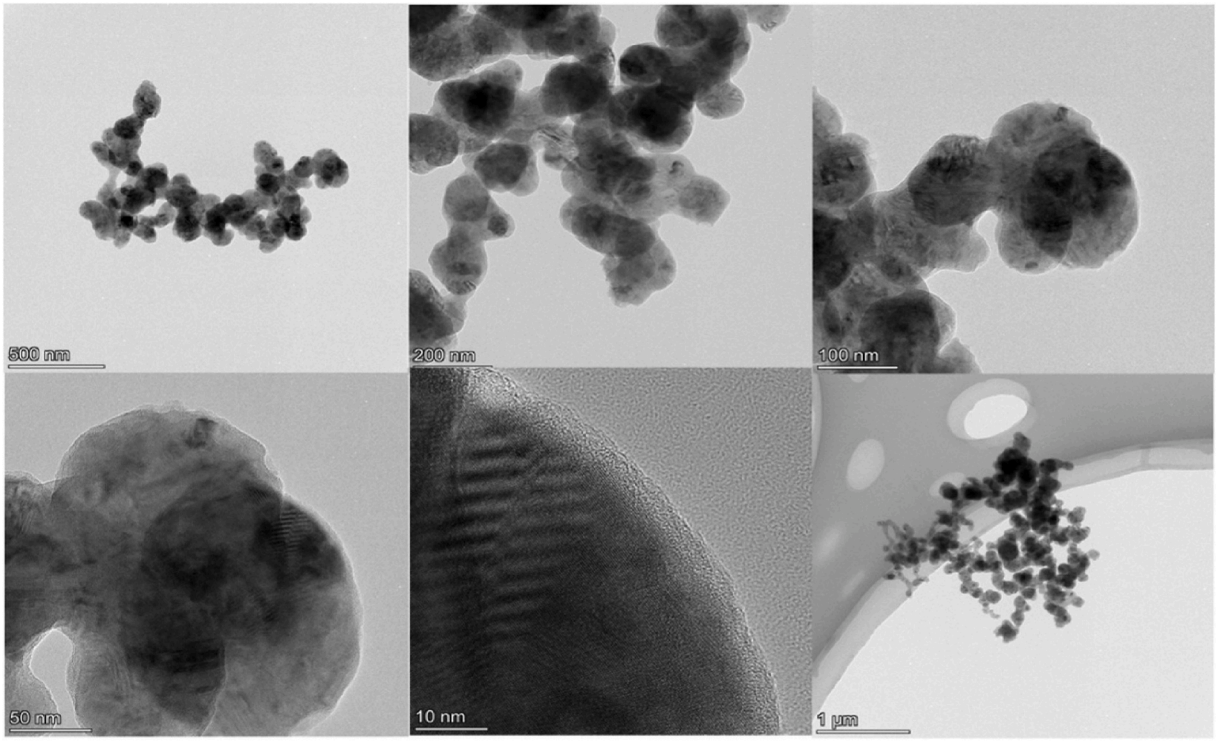

Fig. 3. Transmission electron microscopy (TEM) images of green synthesized silicon nanoparticles (GS-SiNPs), magnified at the accelerating voltage of 200 KV, camera length of 520 mm, and electron wavelength of 0.0251 Å.

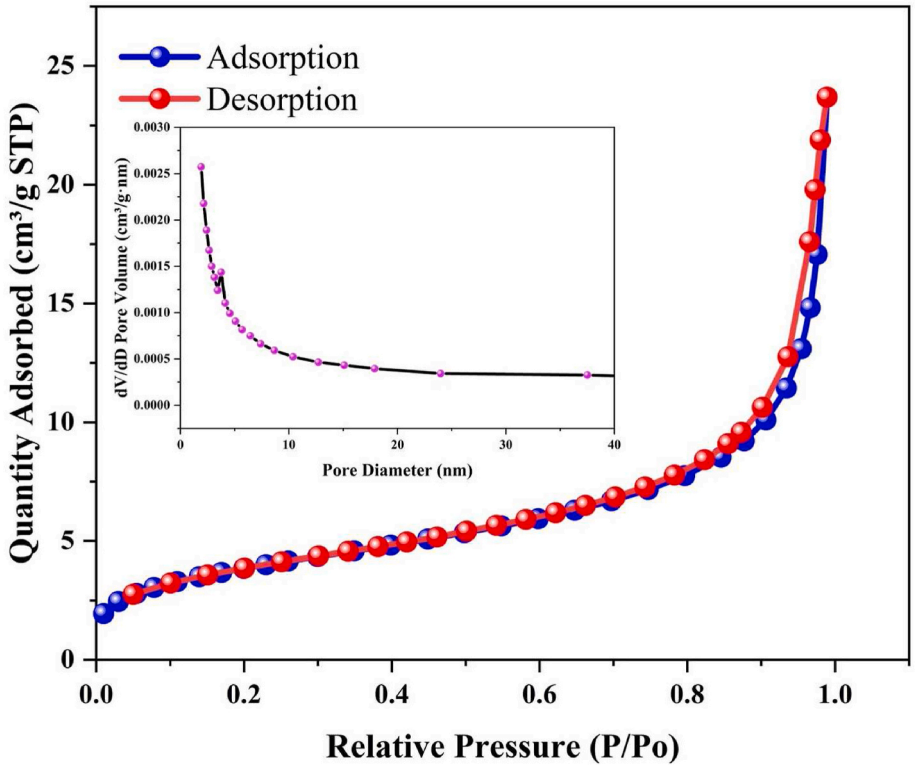

Fig. 4. N_2 adsorption-desorption isotherm of green synthesized silicon nanoparticles (GS-SiNPs): the inset shows the pore size distribution. (For interpretation of the references to colour in this figure legend, the reader is referred to the Web version of this article.)

1634 and 3442 cm^{-1} are due to N–H stretching and bending, respectively (Nieto et al., 2008). For the case of peaks after adsorption of Cr (VI) on GS-SiNPs, an additional peak appeared at 1240 cm^{-1} occurs, the band at 1240 cm^{-1} belong to the secondary –OH bending vibrations (Rajagopal et al., 2021). These outcomes reveal the role of distinct functional groups for the reduction and stabilization of the GS-SiNPs.

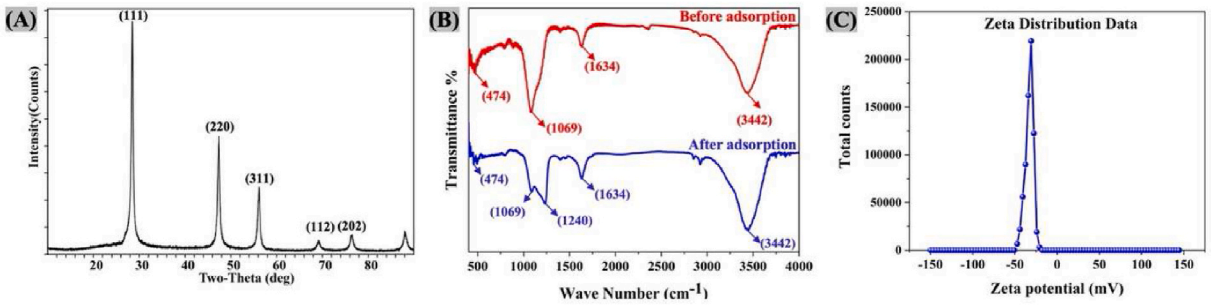

Fig. 5. XRD patterns (A), FTIR spectra before and after Cr (VI) adsorption (B), and Zeta potential (C) of green synthesized silicon nanoparticles (GS-SiNPs). (For interpretation of the references to colour in this figure legend, the reader is referred to the Web version of this article.)

Furthermore, the surface charge of GS-SiNPs and SiNPs was examined by Zeta potential (Fig. 5C and S1, respectively). The results showed that the surface charge of GS-SiNPs was −32.9 mV and the zeta deviation was 4.79 mV (Alvarez-Berrios et al., 2018; Sharma et al., 2021; Song et al., 2005), which shows the stability of GS-SiNPs (Kim et al., 2014b). The presence of a negative charge on the surface of GS-SiNPs corresponds to Si–OH groups (Sharma et al., 2021), since these Si–OH groups are deprotonated to form SiO- species in water, resulting in the formation negative charges on the surface of SiNPs (Kim et al., 2014a).

3.2. Effect of pH

It must be noted that the pH of the solution is a critical factor in the adsorption process, one which both affects the surface charge of any adsorbent and influences the species of metal ions (Ahmed et al., 2021b). The pH of the aqueous solution affects the solubility of the metal ions, concentration of the counter ions on the functional groups on the sorbent and the degree of the ionization of the sorbent during the adsorption process (Anah and Astrini, 2017). The effect of this parameter on the removal of Cr (VI) was analyzed by varying the pH of the solution from 2 to 7 (Fig. 6A). As discussed earlier, a specific dose (100 mg L^{-1}) and a specific contact time (60 min) were selected to study the

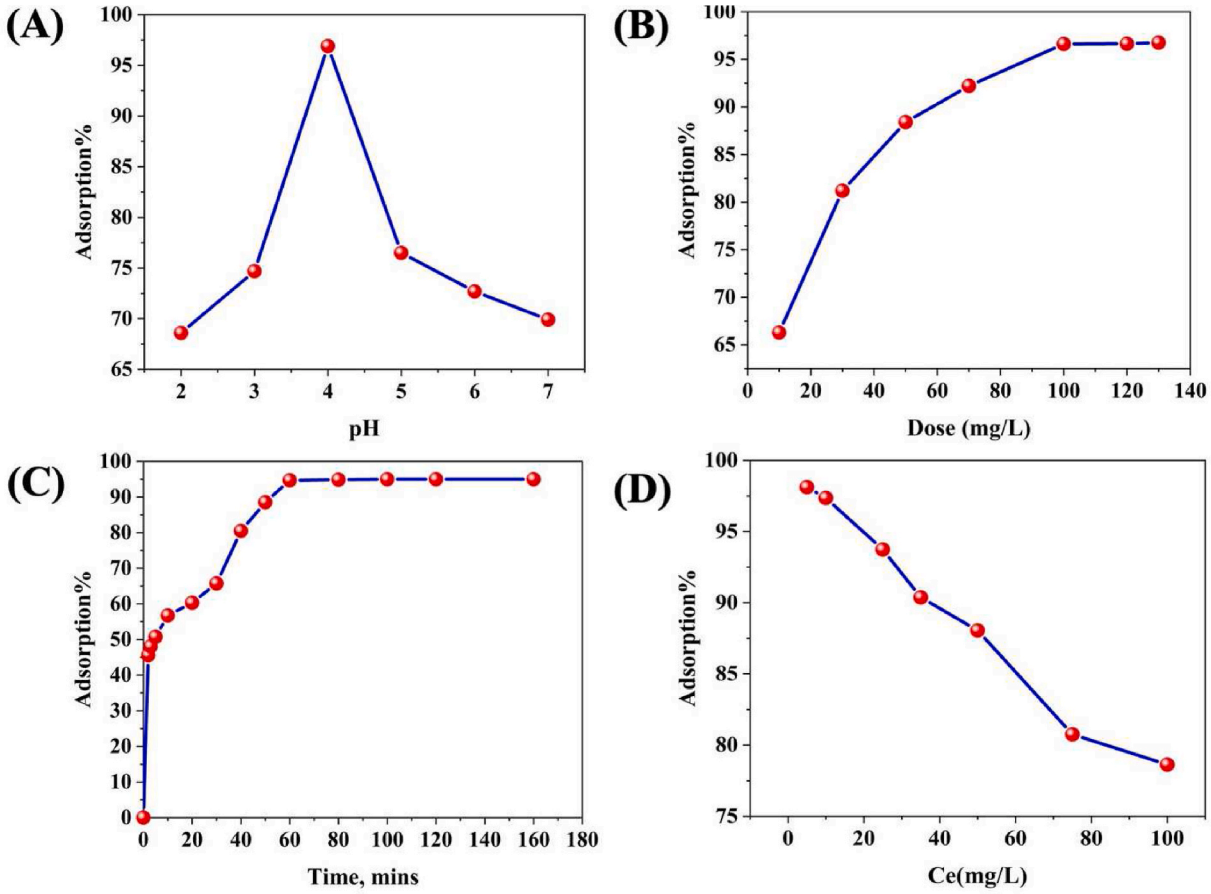

Fig. 6. (A) Effect of pH on the adsorption capacity of 50 mg L^{-1} Cr (VI) in the presence of 100 mg L^{-1} of GS-SiNPs at 25 °C and with contacting time of 60 min. (B) Removal percent of Cr (VI) (50 mg L^{-1}) as a function of 100 mg L^{-1} GS-SiNPs dose at pH 4.0 ambient temperature 25 °C and with contacting time of 60 min. (C) Effect of contact time on the adsorption capacity of 50 mg L^{-1} Cr (VI) at pH 4 in the presence of 100 mg L^{-1} of GS-SiNPs at 25 °C. (D) Removal percent of Cr (VI) at different concentrations at pH 4 in the presence of 100 mg L^{-1} of GS-SiNPs at 25 °C with contacting time of 60 min. Average values (n = 3), with coefficients of variation always lower than 5%.

effect of the pH of the solution, alongside the initial concentration of 50 mg L^{-1} for Cr (VI). The highest removal efficiency (96.9%) of Cr (VI) by GS-SiNPs was recorded at pH 4.0 (Fig. 6A). These results can be explained by the multiple phenomena involved in this system, such as reduction of Cr (VI), adsorption/desorption of chromium ions, and protonation/deprotonation of cell wall functional groups depending on solution pH (Silva et al., 2009). The balance of protonation and deprotonation depended on the pH of the solution and the pHpzc of adsorbent (Ghorbel-Abid et al., 2016). It was noted that the removal efficiency of Cr (VI) by GS-SiNPs was higher under acidic conditions, and lower under neutral conditions, which in fact could be attributed to the variation of pH (Kekes et al., 2021). At a pH value in the range 3.0–6.0, the Cr (VI) ions exist in the form of $HCrO_4^-$, H_2Cr_4, and $Cr_2O_7^{2-}$ (Yao et al., 2020), whilst, at a pH value in the range 6.0–12.0, the Cr (VI) ions are mainly available as CrO_4^{2-}, which is found to be difficult to reduce compared with the other forms of Cr (VI) (Kekes et al., 2021; Zhang et al., 2019). Our findings also confirmed this fact as we found that the lowest Cr (VI) removal efficiency by GS-SiNPs was recorded at pH 2 and 7 (Fig. 6A). The results indicate that pH has an influence on adsorption for Cr(VI), and the optimal pH value for Cr(VI) adsorption is 4.0 (Zhang et al., 2020).

3.3. Effect of adsorbent dose

The study also investigated the effect of varying doses of GS-SiNPs on the removal of Cr (VI) (Fig. 6B). The dose of GS-SiNPs varied from 10 to 130 mg L^{-1} during the experiment, while maintaining a constant contact time of 60 min, on account of the maximum Cr (VI) adsorption on GS-SiNPs that was found to occur in this timeframe. The results in Fig. 6B show that the removal rate increased with the increase of GS-SiNPs dose. When the dose increased from 10 to 130 mg L^{-1}, the removal rate for Cr (VI) increased substantially. On further increasing of adsorbent dose, the increase of removal rate was not significant. The highest removal rate reached 96.76% for Cr (VI) respectively. Considering factors of removal efficiency and economic cost, 100 mg L^{-1} was taken as the optimum dose in further studies. The removal capacity of the adsorbent increased with increasing adsorbent dose (Fig. 6B), which could be attributed to the availability of a larger number of active sites on the adsorbent surface (Ahmed et al., 2021a; Sharma et al., 2021). Previous studies suggested that increases in the mass of the adsorbent can lead to increases in its surface area and adsorption potential (Younis et al., 2020). On the other hand, it could be concluded from Fig. 7, that as the initial concentration of adsorbent raises from 10 to 130 mg L^{-1} the adsorption capacity declines from 3.91 to 0.52 mg g^{-1}. The reason is that when the initial concentration of adsorbent is increased, a larger area becomes exposed to Cr (VI) ion adsorption and as a result the Cr (VI) ions face more competition to fill the actives sites and it results in lots of active sites on the surface of adsorbent to remain unsaturated and the adsorption capacity to decrease (Chabaane et al., 2011). The removal rate also was above 96.63% in 100 mg L^{-1} adsorbent solution, while the adsorption capacity was reduced, which can be explained by the increase in available adsorption sites at a certain contaminant concentration (Gao et al., 2019). According to the obtained results a dosage of 100 mg L^{-1} was selected as the optimum initial concentration of the adsorbent.

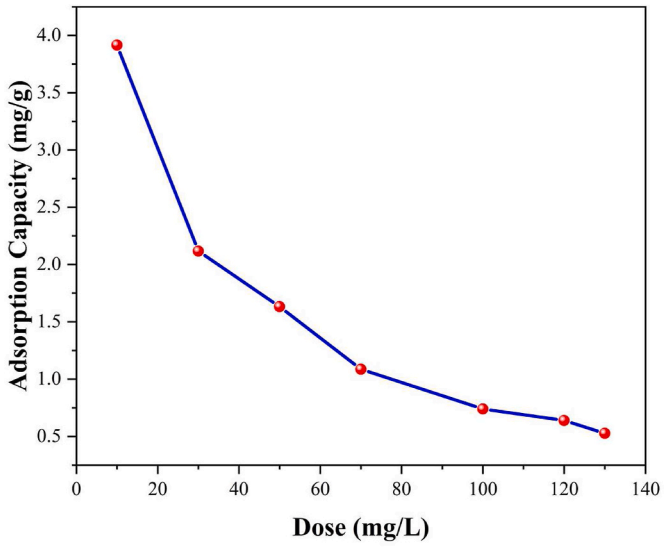

Fig. 7. Effect of adsorbent dosage on the amount of Cr (VI) adsorbed per gram of adsorbent at room temperature.

3.4. The effect of co-existing ions

Moreover, in this study, the influence of coexisting common ions was performed with cations (Na^+, K^+, Mg^{2+}, Ca^{2+}) and anions (Cl^-, NO_3^-, CO_3^{2-}, SO_4^{2-}) at a concentration of 0.1 M for each (Zhang et al., 2020). As shown in Fig. 8, the adsorption capacity of GS-SiNPs showed a trend to be maintained even in the co-existence of different ions, suggesting that their presence have no significant effect on the adsorption capacity of GS-SiNPs towards Cr (VI) removal (Ahmed et al., 2021b). According to Hu et al. (2005) the common ions coexisting in solution invariably compete with Cr (VI) for the limited adsorption sites of maghemite nanoparticle adsorbent. Such impacts need future further studies, as other transition metal ions could influence the Cr (VI) removal from wastewater.

3.5. Isotherm and kinetics analysis

The kinetics data were fitted by pseudo-first-order and pseudo-second-order kinetics according to equations (5) and (6) (Poguberović et al., 2016), and the results are listed in Table 1. Results in Table 1 indicate that qe in the pseudo-second-order model was more consistent, and the coefficients (R^2) in pseudo-second-order kinetics were larger than 90% (see Table 2).

The effect of contact time on the adsorptive removal of Cr (VI) using GS-SiNPs was investigated by plotting the removal percentage of Cr (VI)

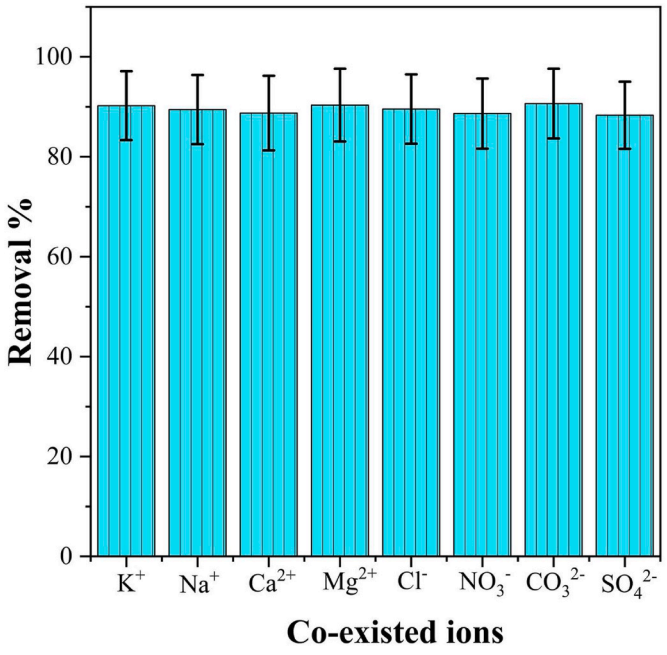

Fig. 8. Effect of common cations and anions on Cr (VI) removal.

Table 1
Experimentally determined kinetic, Langmuir and Freundlich parameters for Cr (VI) adsorption by green synthesized silicon nanoparticles (GS-SiNPs).

Metric	GS-SiNPs		
Initial Cr concentration	50 ppm		
Contact time	60 min		
pH	4.0		
Dosage	100 mg		
Langmuir isotherm	Q_m = 2.55 (mg g^{-1})	K_L = 0.558 (L mg^{-1})	R^2 (%) = 94.80
Freundlich isotherm	n = 1.3713	K_F = 7.614 (mg g^{-1})	R^2 (%) = 97.79
Pseudo-first order	Q_e (mg g^{-1}) = 1.13	K_1 (1/min) = 0.000079	R^2 (%) = 85.69
Pseudo-second order	Q_e (mg g^{-1}) = 3.28	K_2 (g mg^{-1} min^{-1}) = 0.192461	R^2 (%) = 90.68

Table 2
Comparison of the maximum adsorption capacities of Cr (VI) obtained in this study and those reported in other studies.

Adsorbents	Qm (mg g^{-1})	References
Zeolites modified ZVI	2.49	Dang et al., (2014)
Magnetite–maghemite nanoparticles	2.40	Chowdhury and Yanful (2010)
Magnetic carbon nanocomposite	3.7	Zhu et al., (2014)
Magnetite nanoparticles	3.81	Huang et al., (2015) Di et al., (2006)
Olive stones coated by iron-based nanoparticles	5.78	Vilardi et al., (2018)
Amorphous silica nanoparticles	0.4	Jang et al., (2020)
Green synthesized CuO nanoparticles	16.63	Mohan et al., (2015)
Ceria nanoparticles	1.5	Di et al., (2006)
Green synthesized iron nanoparticles	20.5	Jin et al., (2018)
Synthesized CeO2 nanoparticles	1.88	Recillas et al., (2010)
Mesoporous silica nanoparticles	1.3	Jang et al., (2020)
Green synthesized silicon nanoparticle	2.55	This study

against the contact time (Fig. 6C). The adsorption kinetic experiments were carried out in Cr (VI) concentrations of 50 mg L^{-1}. The GS-SiNPs dose was 100 mg L^{-1}, and the pH of the water was 4.0. Samples were taken at different times to determine the residual concentrations of Cr (VI). A sharp increase in the adsorption of Cr (VI) was noticed during the initial 20 min, before it became stable at 60 min. The functional groups and active available sites on the surface of GS-SiNPs could be responsible for the adsorption of Cr (VI). Meanwhile, the increase in the adsorption rate during the initial minutes could be attributed to strong surface complexation of Cr (VI) with functional groups, which is more probable than the phenomenon of physical adsorption (Sun et al., 2012). Moreover, pseudo-first and second order kinetic models were employed to gain further understanding of the adsorption kinetics of Cr (VI) on GS-SiNPs (Fig. 9A and B). The calculated values of the relevant kinetic parameters are listed in Table 1. The adsorption data for GS-SiNPs fitted the pseudo-second order kinetic model, indicating that chemical adsorption may be involved in the adsorption of Cr (VI), and that it may involve valence forces, with electrons being shared between the adsorbents and the metal cations (Ahmed et al., 2021b). This indicates that the adsorption process was well accordant with the pseudo-second-order reaction (Rajput et al., 2016). The Q_e value of GS-SiNPs was recorded to be 3.28 mg g^{-1}.

To gain a comprehensive understanding of the adsorption of Cr (VI) by GS-SiNPs, the collected data were used for fitting to Langmuir and Freundlich isotherm models (Fig. 9C and D and Table 1). In this section, the initial concentrations of Cr (VI) were controlled at 50 mg L^{-1}, the GS-SiNPs dose was 100 mg L^{-1}, the temperature was 25 ± 2 °C, and the pH of water was 4.0. The adsorption isotherms were fitted according to the linear form of the Langmuir isotherm equation (Equation (3)) and the linear form of Freundlich isotherms equation (Equation (4)) (Boparai et al., 2011). The results are shown in Table 1. The adsorption results revealed a good fitting for both the Langmuir and the Freundlich models, for GS-SiNPs. To note that, n being the exponential coefficient of the Freundlich model, a smaller 1/n ratio has been found to lead to better adsorption performance (Kekes et al., 2021); where 1/n is between 0.1 and 0.5, it indicates that the adsorption reaction is effective, while a value of 1/n greater than 2.0 indicates that the adsorption reaction is low. In this study, 1/n was 0.7038, indicating that the adsorption reaction was favorable. It was also observed that the adsorption of Cr (VI) on the surface of GS-SiNPs was a monolayer process, and that the GS-SiNPs had a homogeneous adsorption surface. The maximum adsorption capacity of GS-SiNPs was 2.55 mg g^{-1}. The sorption performance of GS-SiNPs indicated that it could be a promising option for removing Cr (VI) from polluted waters.

3.6. Possible adsorption mechanisms

The pseudo-second-order model fitting results for chromium (Cr (VI)) sorption kinetics suggested that chemisorption was involved in the Cr (VI) sorption on GS-SiNPs. Previous studies have reported that sorption of Cr (VI) might involve many different interactions, such as electrostatic interaction, hydrophobic interaction, ligand and ion exchange, and hydrogen bond (Badruddoza et al., 2017; Jain et al., 2018; Liu et al., 2019). Further Choi et al. (2018) also reported that the adsorption of Cr (VI) was affected by the solution pH and altered the nanoparticle surface chemically. First principles calculations of the adsorption energies for the relevant adsorption configurations and XPS peaks of Cr showed that Cr (VI) is reduced to Cr (III), by an amine group and that Cr (III) and Cr (VI) ions are adsorbed on different functional groups. Our data suggest that the Langmuir model adequately quantify the maximum equilibrium binding capacity and thus removal efficiency of Cr (VI) onto GS-SiNPs. Further, the Langmuir model as a relevant model for nanoparticles mediated Cr (VI) removal has been widely applied in previous studies (Jain et al., 2018; Liu et al., 2019; Sorwat et al., 2020). Post adsorption FTIR of the GS-SiNPs (Fig. 5B) showed adsorption of chromium due to the functional groups on the surface of GS-SiNPs. After the adsorption of Cr (VI) on GS-SiNPs, an additional peak appeared at 1240 cm^{-1} which corresponds to the presence of C–H groups (Azarshin et al., 2017) and shows the involvement of carboxylate group in Cr (VI) adsorption and surface complexation and this result is in agreement with previous studies (Choudhary et al., 2017; Xu et al., 2018). To further investigate the mechanism of Cr (VI) adsorption onto GS-SiNPs, XPS analysis was performed. The XPS spectra of GS-SiNPs and Cr (VI)-loaded GS-SiNPs are shown in Fig. 10A–E. The survey scans of GS-SiNPs before and after the adsorption of Cr (VI) are shown in Fig. 10A. Similar characteristic peaks assigned to C 1s, O 1s and Si 2p are present on both spectra. The existence of a Cr (VI) 2p peak at 576.29 eV after adsorption serves as evidence of the retention of Cr (VI) ions (Wan et al., 2019) on GS-SiNPs. Furthermore, we can infer the interaction mechanisms from the C 1s (B), O 1s (C), Si 2p (D) spectra analysis, both before and after Cr (VI) adsorption. The fitting of the Si 2p peaks in GS-SiNPs exhibits Si $2p_{3/2}$ and Si 2p at 102.7 eV and 99.0 eV, respectively. This is further confirmed by O 1s spectra, which exhibit three peaks at 532.7 eV, 533.2 eV, and 534.6 eV, corresponding to Si–O–Si, Si–OH and O–H, respectively (Moulder et al., 1993; Sharma et al., 2021). Both the relative proportions and the positions of these O-donor functional groups exhibit variations after Cr (VI) adsorption. After metal sorption, these were primarily attributed to the reduction of the electron cloud density around oxygen (Cai et al., 2019). The C 1s spectra fitted with three peaks corresponds to C–C (284.6 eV), C–O (285.4 eV) and C═O (288.5 eV) bonds, which are similar results to those from other studies (Ahmed et al., 2021b; Sharma et al., 2021). Moreover, C 1s was observed to exhibit significant changes after Cr (VI) adsorption. Fig. 11 further explained the adsorption of Cr (VI) on the surface of GS-SiNPs. The above results of XPS spectra before and after Cr (VI) adsorption

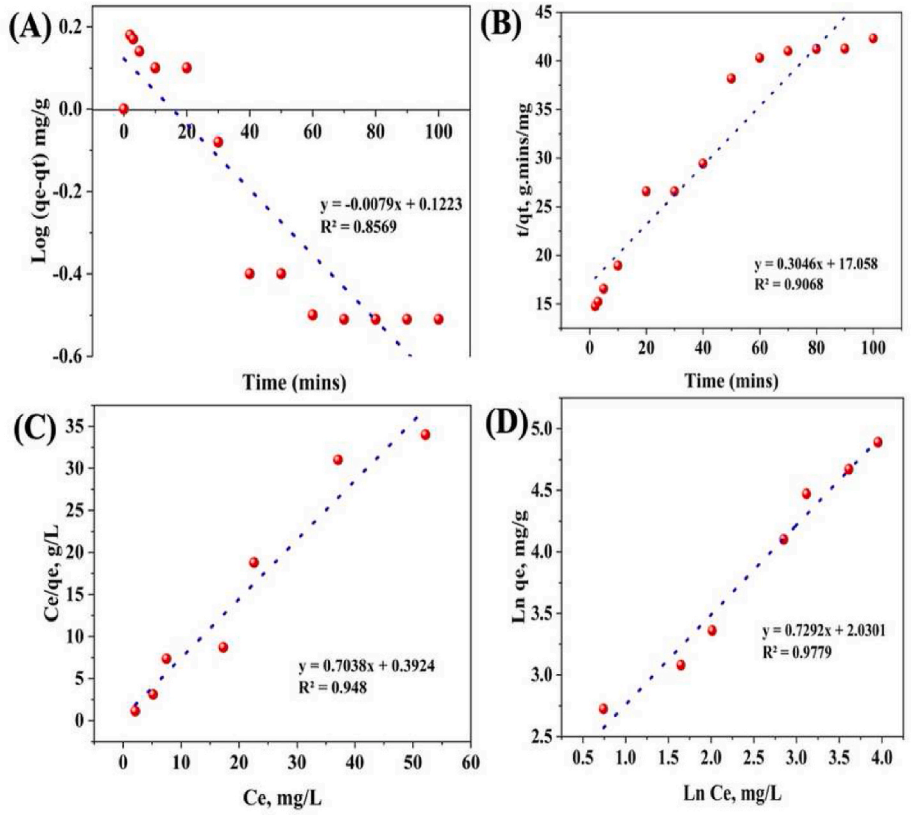

Fig. 9. Pseudo-first order (A), Pseudo-second order (B), Langmuir adsorption isotherm plot (C), and Freundlich adsorption isotherm plot (D) of Cr (VI) on green synthesized silicon nanoparticles (GS-SiNPs). (For interpretation of the references to colour in this figure legend, the reader is referred to the Web version of this article.)

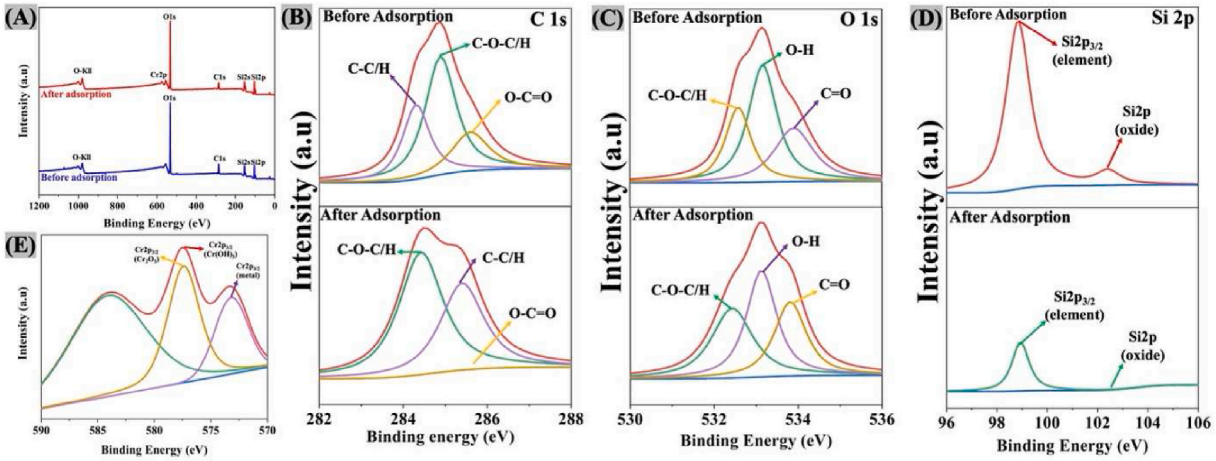

Fig. 10. Survey scan (A), C1s (B), O1s (C), Si2p (D), and Cr2p (E) spectra of green synthesized silicon nanoparticles (GS-SiNPs) before and after adsorption of Cr (VI). (For interpretation of the references to colour in this figure legend, the reader is referred to the Web version of this article.)

clearly indicate "surface complexation" between Cr (VI) and different functional groups (–COOH and –OH) as possible phenomena that subsidized to aqueous Cr (VI) removal. Hence, the green synthesized silicon nanoparticles (GS-SiNPs) could be an affective adsorbent for Cr (VI) (and maybe other heavy metals) removal from contaminated environments.

3.7. Recyclability of green synthesized silicon nanoparticles

The recyclability of catalyst is a great advantage in reducing the overall cost in process chemistry and decreasing environmental pollution. It eliminates involvement in the synthesis and resale process. The Cr (VI) concentrations was 50 mg L^{-1}, and the adsorbent dose was 100 mg L^{-1}. The pH of the water was 4.0. The adsorption stability of GS-SiNPs was investigated for the reusability test, as shown in Fig. 12. Even though there were six cycles, there was no significant loss of adsorption activity, showing that the adsorbent was stable and reusable.

4. Conclusion

In the current study, SiNPs were synthesized from horsetail

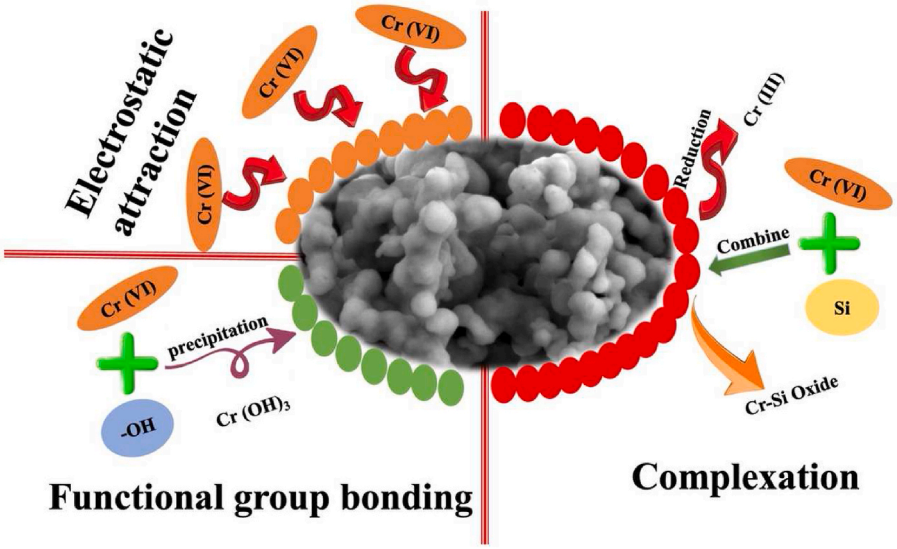

Fig. 11. Possible adsorption mechanism of Cr adsorption on the surface of green synthesized silicon nanoparticles (GS-SiNPs). (For interpretation of the references to colour in this figure legend, the reader is referred to the Web version of this article.)

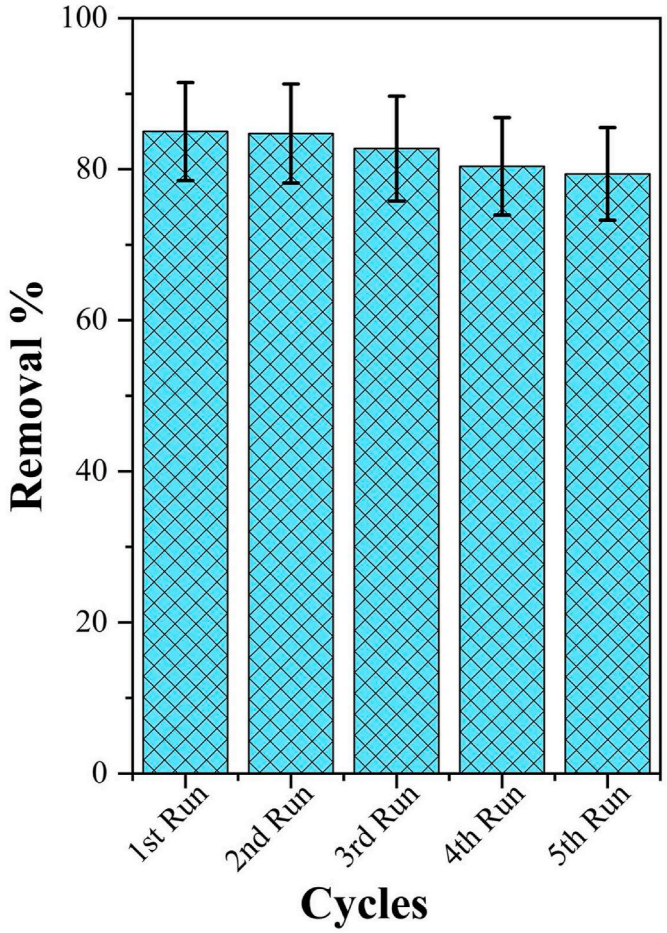

Fig. 12. Regeneration studies of GS-SiNPs for the removal of Cr (VI).

(*Equisetum arvense*) plants and characterized by FTIR, SEM-EDX, BET, XRD, TEM, and XPS techniques. Green synthesized silicon nanoparticles (GS-SiNPs) were found to effectively remove Cr (VI) under different experimental conditions (such as varying pH, contact time, and dosage). The GS-SiNPs nanoparticles showed good adsorption capacity for Cr (VI) in water and can be reused stably. At concentrations of Cr (VI) at 50 mg L^{-1}, and with a GS-SiNPs dose of 100 mg L^{-1}, the maximum adsorption capacity was reached to 2.55 mg g^{-1}. The adsorption capacity of GS-SiNPs for Cr (VI) was strongly dependent on pH, and the removal rate was higher when pH was 4.0. The adsorption capacity increased with the increase of the initial Cr (VI) concentration in water, while the removal rate decreased with the increase of the initial Cr (VI) concentrations. The increase of GS-SiNPs dose improved the adsorption efficiencies for Cr (VI). The adsorption process fitted well the Langmuir and Freundlich isotherms of Cr (VI) adsorption. The maximum adsorption capacity of GS-SiNPs was 2.55 mg g^{-1}. The common coexisting anions and cations had no effect on the adsorption of Cr (VI). The results of this study show that GS-SiNPs are effective adsorbents and can enhance the removal of water pollutants (specifically Cr (VI)), which would have great environmental and economic benefits in the future.

Declaration of competing interest

The authors declare that they have no known competing financial interests or personal relationships that could have appeared to influence the work reported in this paper.

Acknowledgement

The National Natural Science Foundation of China (NSFC-31860728) financially supported this research.

Appendix A. Supplementary data

Supplementary data to this article can be found online at https://doi.org/10.1016/j.envres.2022.113614.

References

Adinarayana, T.V.S., Mishra, A., Singhal, I., Koti Reddy, D.V.R., 2020. Facile green synthesis of silicon nanoparticles from: equisetum arvense for fluorescence based detection of Fe(iii) ions. Nanoscale Adv. https://doi.org/10.1039/d0na00307g.

Ahmed, W., Mehmood, S., Núñez-Delgado, A., Qaswar, M., Ali, S., Ying, H., Liu, Z., Mahmood, M., Chen, D.Y., 2021a. Fabrication, characterization and U(VI) sorption properties of a novel biochar derived from Tribulus terrestris via two different approaches. Sci. Total Environ. https://doi.org/10.1016/j.scitotenv.2021.146617.

Ahmed, W., Núñez-Delgado, A., Mehmood, S., Ali, S., Qaswar, M., Shakoor, A., Chen, D. Y., 2021b. Highly efficient uranium (VI) capture from aqueous solution by means of a hydroxyapatite-biochar nanocomposite: adsorption behavior and mechanism. Environ. Res. https://doi.org/10.1016/j.envres.2021.111518.

Ajiboye, T.O., Oyewo, O.A., Onwudiwe, D.C., 2021. Simultaneous removal of organics and heavy metals from industrial wastewater: a review. Chemosphere. https://doi.org/10.1016/j.chemosphere.2020.128379.

Alvarez-Berrios, M.P., Aponte-Reyes, L.M., Aponte-Cruz, L.M., Loman-Cortes, P., Vivero-Escoto, J.L., 2018. Effect of the surface charge of silica nanoparticles on oil recovery: wettability alteration of sandstone cores and imbibition experiments. Int. Nano Lett. https://doi.org/10.1007/s40089-018-0243-5.

Anah, L., Astrini, N., 2017. Influence of pH on Cr(VI) ions removal from aqueous solutions using carboxymethyl cellulose-based hydrogel as adsorbent. In: IOP Conference Series: Earth and Environmental Science. https://doi.org/10.1088/1755-1315/60/1/012010.

Annenkov, V.V., Gordon, R., Zelinskiy, S.N., Danilovtseva, E.N., 2020. The probable mechanism for silicon capture by diatom algae: assimilation of polycarbonic acids with diatoms—is endocytosis a key stage in building of siliceous frustules? J. Phycol. https://doi.org/10.1111/jpy.13062.

Ayawei, N., Ebelegi, A.N., Wankasi, D., 2017. Modelling and interpretation of adsorption isotherms. J. Chem. https://doi.org/10.1155/2017/3039817.

Azarshin, S., Moghadasi, J., A Aboosadi, Z., 2017. Surface functionalization of silica nanoparticles to improve the performance of water flooding in oil wet reservoirs. Energy Explor. Exploit. https://doi.org/10.1177/0144598717716281.

Azimi, A., Azari, A., Rezakazemi, M., Ansarpour, M., 2017. Removal of Heavy Metals from Industrial Wastewaters: A Review. ChemBioEng Rev. https://doi.org/10.1002/cben.201600010.

Badruddoza, A.Z.M., Bhattarai, B., Suri, R.P.S., 2017. Environmentally friendly β-cyclodextrin-ionic liquid polyurethane-modified magnetic sorbent for the removal of PFOA, PFOS, and Cr(VI) from water. ACS Sustain. Chem. Eng. https://doi.org/10.1021/acssuschemeng.7b02186.

Bhat, P.S., Venkatram, R., 2019. Preference towards marketing channels: a case of tomato farmers in Kolar district of Karnataka. Int. J. Farm Sci. https://doi.org/10.5958/2250-0499.2019.00001.6.

Boparai, H.K., Joseph, M., O'Carroll, D.M., 2011. Kinetics and thermodynamics of cadmium ion removal by adsorption onto nano zerovalent iron particles. J. Hazard Mater. https://doi.org/10.1016/j.jhazmat.2010.11.029.

Cai, Y., Wang, X., Feng, J., Zhu, M., Alsaedi, A., Hayat, T., Tan, X., 2019. Fully phosphorylated 3D graphene oxide foam for the significantly enhanced U(VI) sequestration. Environ. Pollut. https://doi.org/10.1016/j.envpol.2019.03.013.

Chabaane, L., Tahiri, S., Albizane, A., Krati, M. El, Cervera, M.L., de la Guardia, M., 2011. Immobilization of vegetable tannins on tannery chrome shavings and their use for the removal of hexavalent chromium from contaminated water. Chem. Eng. J. https://doi.org/10.1016/j.cej.2011.09.037.

Chapa-González, C., Piñón-Urbina, A.L., García-Casillas, P.E., 2018. Synthesis of controlled-size silica nanoparticles from sodium metasilicate and the effect of the addition of PEG in the size distribution. Materials. https://doi.org/10.3390/ma11040510.

Chen, B., Wang, M., Duan, M., Ma, X., Hong, J., Xie, F., Zhang, R., Li, X., 2019. In search of key: protecting human health and the ecosystem from water pollution in China. J. Clean. Prod. https://doi.org/10.1016/j.jclepro.2019.04.228.

Chen, Z., Kahn, M.E., Liu, Y., Wang, Z., 2018. The consequences of spatially differentiated water pollution regulation in China. J. Environ. Econ. Manag. https://doi.org/10.1016/j.jeem.2018.01.010.

Choi, K., Lee, S., Park, J.O., Park, J.A., Cho, S.H., Lee, S.Y., Lee, J.H., Choi, J.W., 2018. Chromium removal from aqueous solution by a PEI-silica nanocomposite. Sci. Rep. https://doi.org/10.1038/s41598-018-20017-9.

Choudhary, B., Paul, D., Singh, A., Gupta, T., 2017. Removal of hexavalent chromium upon interaction with biochar under acidic conditions: mechanistic insights and application. Environ. Sci. Pollut. Res. https://doi.org/10.1007/s11356-017-9322-9.

Chowdhury, S.R., Yanful, E.K., 2010. Arsenic and chromium removal by mixed magnetite-maghemite nanoparticles and the effect of phosphate on removal. J. Environ. Manag. 91, 2238–2247. https://doi.org/10.1016/j.jenvman.2010.06.003.

Codex Alimentarius Commission, 1997. Report of the twenty-second session of the joint FAO/WHO codex Alimentarius commission. ALINORM 97, 37.

Dang, H., Zhang, Y., Du, P., 2014. Enhanced removal of soluble Cr(VI) by using zero-valent iron composite supported by surfactant-modified zeolites. Water Sci. Technol. https://doi.org/10.2166/wst.2014.392.

Di, Z.-C., Ding, J., Peng, X.-J., Li, Y.-H., Luan, Z.-K., Liang, J., 2006. Chromium adsorption by aligned carbon nanotubes supported ceria nanoparticles. Chemosphere 62, 861–865. https://doi.org/10.1016/j.chemosphere.2004.06.044.

Dianyi Yu, M., 2010. Agency for Toxic Substances and Disease Registry Case Studies in Environmental Medicine (CSEM) Trichloroethylene Toxicity. Atsdr.

Egbueri, J.C., 2020. Heavy metals pollution source identification and probabilistic health risk assessment of shallow groundwater in onitsha, Nigeria. Anal. Lett. https://doi.org/10.1080/00032719.2020.1712606.

Egbueri, J.C., Ezugwu, C.K., Ameh, P.D., Unigwe, C.O., Ayejoto, D.A., 2020. Appraising drinking water quality in Ikem rural area (Nigeria) based on chemometrics and multiple indexical methods. Environ. Monit. Assess. https://doi.org/10.1007/s10661-020-08277-3.

El-Saadony, M.T., Desoky, E.S.M., Saad, A.M., Eid, R.S.M., Selem, E., Elrys, A.S., 2021. Biological silicon nanoparticles improve Phaseolus vulgaris L. yield and minimize its contaminant contents on a heavy metals-contaminated saline soil. J. Environ. Sci. (China). https://doi.org/10.1016/j.jes.2021.01.012.

Farajzadeh Memari-Tabrizi, E., Yousefpour-Dokhanieh, A., Babashpour-Asl, M., 2021. Foliar-applied silicon nanoparticles mitigate cadmium stress through physio-chemical changes to improve growth, antioxidant capacity, and essential oil profile of summer savory (Satureja hortensis L.). Plant Physiol. Biochem. https://doi.org/10.1016/j.plaphy.2021.04.040.

Ferrari, M., 2005. Ferrari, M. Cancer Nanotechnology: Opportunities and Challenges. Nat. Rev. Cancer 5. Nat. Rev. Cancer, pp. 161–171.

Gao, H., Du, J., Liao, Y., 2019. Removal of chromium(VI) and orange II from aqueous solution using magnetic polyetherimide/sugarcane bagasse. Cellulose. https://doi.org/10.1007/s10570-019-02301-7.

García-Gaytán, V., Bojórquez-Quintal, E., Hernández-Mendoza, F., Tiwari, D.K., Corona-Morales, N., Moradi-Shakoorian, Z., 2019. Polymerized silicon (SiO2·nH2O) in Equisetum arvense: potential nanoparticle in crops. J. Chil. Chem. Soc. https://doi.org/10.4067/s0717-97072019000104298.

Ghorbel-Abid, I., Vagner, C., Denoyel, R., Trabelsi-Ayadi, M., 2016. Effect of cadmium and chromium adsorption on the zeta potential of clays. Desalination Water Treat. https://doi.org/10.1080/19443994.2015.1134350.

Gupta, A., Wiggers, H., 2011. Freestanding silicon quantum dots: origin of red and blue luminescence. Nanotechnology. https://doi.org/10.1088/0957-4484/22/5/055707.

Hu, J., Chen, G., Lo, I.M.C., 2005. Removal and recovery of Cr(VI) from wastewater by maghemite nanoparticles. Water Res. https://doi.org/10.1016/j.watres.2005.05.051.

Hu, J., Lo, I.M.C., Chen, G., 2007. Comparative study of various magnetic nanoparticles for Cr(VI) removal. Separ. Purif. Technol. https://doi.org/10.1016/j.seppur.2007.02.009.

Huang, S., Pang, H., Li, L., Jiang, S., Wen, T., Zhuang, L., Hu, B., Wang, X., 2018. Unexpected ultrafast and high adsorption of U(VI) and Eu(III) from solution using porous Al2O3 microspheres derived from MIL-53. Chem. Eng. J. https://doi.org/10.1016/j.cej.2018.07.129.

Huang, Z., nan, Wang, ling, X., Yang, D. suo, 2015. Adsorption of Cr(VI) in wastewater using magnetic multi-wall carbon nanotubes. Water Sci. Eng. https://doi.org/10.1016/j.wse.2015.01.009.

Iqbal, M., Purkait, T.K., Goss, G.G., Bolton, J.R., Gamal El-Din, M., Veinot, J.G.C., 2016. Application of engineered Si nanoparticles in light-induced advanced oxidation remediation of a water-borne model contaminant. ACS Nano. https://doi.org/10.1021/acsnano.6b01619.

Irfan, M., Ishaq, F., Muhammad, D., Khan, M.J., Mian, I.A., Dawar, K.M., Muhammad, A., Ahmad, M., Anwar, S., Ali, S., Khan, F.U., Khan, B., Bibi, H., Kamal, A., Musarat, M., Ullah, W., Saeed, M., 2021. Effect of wheat straw derived biochar on the bioavailability of Pb, Cd and Cr using maize as test crop. J. Saudi Chem. Soc. https://doi.org/10.1016/j.jscs.2021.101232.

Jain, M., Yadav, M., Kohout, T., Lahtinen, M., Garg, V.K., Sillanpää, M., 2018. Development of iron oxide/activated carbon nanoparticle composite for the removal of Cr(VI), Cu(II) and Cd(II) ions from aqueous solution. Water Resour. Ind. https://doi.org/10.1016/j.wri.2018.10.001.

Jang, E.H., Pack, S.P., Kim, I., Chung, S., 2020. A systematic study of hexavalent chromium adsorption and removal from aqueous environments using chemically functionalized amorphous and mesoporous silica nanoparticles. Sci. Rep. https://doi.org/10.1038/s41598-020-61505-1.

Jin, X., Liu, Y., Tan, J., Owens, G., Chen, Z., 2018. Removal of Cr(VI) from aqueous solutions via reduction and absorption by green synthesized iron nanoparticles. J. Clean. Prod. https://doi.org/10.1016/j.jclepro.2017.12.026.

Jose, A.R., Sivasankaran, U., Menon, S., Kumar, K.G., 2016. A silicon nanoparticle based turn off fluorescent sensor for Sudan i. Anal. Methods. https://doi.org/10.1039/c6ay01125j.

Kekes, T., Kolliopoulos, G., Tzia, C., 2021. Hexavalent chromium adsorption onto crosslinked chitosan and chitosan/β-cyclodextrin beads: novel materials for water decontamination. J. Environ. Chem. Eng. https://doi.org/10.1016/j.jece.2021.105581.

Kim, K.M., Kim, H.M., Choi, M.H., Lee, J.K., Jeong, J., Lee, M.H., Kim, Y.S., Paek, S.M., Oh, J.M., 2014a. Colloidal properties of surface coated colloidal silica nanoparticles in aqueous and physiological solutions. Sci. Adv. Mater. https://doi.org/10.1166/sam.2014.1837.

Kim, K.M., Kim, H.M., Lee, W.J., Lee, C.W., Kim, T. Il, Lee, J.K., Jeong, J., Paek, S.M., Oh, J.M., 2014b. Surface treatment of silica nanoparticles for stable and charge-controlled colloidal silica. Int. J. Nanomed. https://doi.org/10.2147/IJN.S57922.

Limbach, L.K., Bereiter, R., Müller, E., Krebs, R., Gälli, R., Stark, W.J., 2008. Removal of oxide nanoparticles in a model wastewater treatment plant: influence of agglomeration and surfactants on clearing efficiency. Environ. Sci. Technol. https://doi.org/10.1021/es800091f.

Liu, Y.L., Li, Y.T., Huang, J.F., Zhang, Y.L., Ruan, Z.H., Hu, T., Wang, J.J., Li, W.Y., Hu, H.J., Jiang, G.B., 2019. An advanced sol–gel strategy for enhancing interfacial reactivity of iron oxide nanoparticles on rosin biochar substrate to remove Cr(VI). Sci. Total Environ. https://doi.org/10.1016/j.scitotenv.2019.07.021.

Lou, J., Yu, S., Feng, L., Guo, X., Wang, M., Branco, A.T., Li, T., Lemos, B., 2021. Environmentally induced ribosomal DNA (rDNA) instability in human cells and populations exposed to hexavalent chromium [Cr (VI)]. Environ. Int. https://doi.org/10.1016/j.envint.2021.106525.

Mohan, S., Singh, Y., Verma, D.K., Hasan, S.H., 2015. Synthesis of CuO nanoparticles through green route using Citrus limon juice and its application as nanosorbent for Cr(VI) remediation: process optimization with RSM and ANN-GA based model. Process Saf. Environ. Protect. https://doi.org/10.1016/j.psep.2015.05.005.

Mohd, N.K., Wee, N.N.A.N., Azmi, A.A., 2017. Green synthesis of silica nanoparticles using sugarcane bagasse. In: AIP Conference Proceedings. https://doi.org/10.1063/1.5002317.

Moulder, J.F., Stickle, W.F., Sobol, P.E., Bomben, K.D., 1993. Handbook of X-Ray Photoelectron Spectroscopy. Google Sch.

Muleya, E., Nyomombe, T., Maphosa, N.S., Matunhu, V., 2020. Assessing water quality and its relationship to selected disease patterns in Zvishavane Town, Zimbabwe. J. Appl. Sci. Environ. Manag. https://doi.org/10.4314/jasem.v23i11.21.

Naikoo, G.A., Mustaqeem, M., Hassan, I.U., Awan, T., Arshad, F., Salim, H., Qurashi, A., 2021. Bioinspired and green synthesis of nanoparticles from plant extracts with antiviral and antimicrobial properties: a critical review. J. Saudi Chem. Soc. https://doi.org/10.1016/j.jscs.2021.101304.

Nieto, A., Balas, F., Colilla, M., Manzano, M., Vallet-Regí, M., 2008. Functionalization degree of SBA-15 as key factor to modulate sodium alendronate dosage. Microporous Mesoporous Mater. https://doi.org/10.1016/j.micromeso.2008.03.025.

Philippou, K., Anastopoulos, I., Dosche, C., Pashalidis, I., 2019. Synthesis and characterization of a novel Fe3O4-loaded oxidized biochar from pine needles and its application for uranium removal. Kinetic, thermodynamic, and mechanistic analysis. J. Environ. Manag. https://doi.org/10.1016/j.jenvman.2019.109677.

Poguberović, S.S., Krčmar, D.M., Maletić, S.P., Kónya, Z., Pilipović, D.D.T., Kerkez, D.V., Rončević, S.D., 2016. Removal of As(III) and Cr(VI) from aqueous solutions using "green" zero-valent iron nanoparticles produced by oak, mulberry and cherry leaf extracts. Ecol. Eng. https://doi.org/10.1016/j.ecoleng.2016.01.083.

Rajagopal, G., Nivetha, A., Ilango, S., Muthudevi, G.P., Prabha, I., Arthimanju, R., 2021. Phytofabrication of selenium nanoparticles using Azolla pinnata: evaluation of catalytic properties in oxidation, antioxidant and antimicrobial activities. J. Environ. Chem. Eng. 9 https://doi.org/10.1016/j.jece.2021.105483.

Rajput, S., Pittman, C.U., Mohan, D., 2016. Magnetic magnetite (Fe3O4) nanoparticle synthesis and applications for lead (Pb2+) and chromium (Cr6+) removal from water. J. Colloid Interface Sci. https://doi.org/10.1016/j.jcis.2015.12.008.

Recillas, S., Colón, J., Casals, E., González, E., Puntes, V., Sánchez, A., Font, X., 2010. Chromium VI adsorption on cerium oxide nanoparticles and morphology changes during the process. J. Hazard Mater. https://doi.org/10.1016/j.jhazmat.2010.08.052.

Roychoudhury, A., 2020. Silicon-nanoparticles in crop improvement and agriculture. Int. J. Recent Adv. Biotechnol. Nanotechnol.

Saravanan, A., Kumar, P.S., Karishma, S., Vo, D.V.N., Jeevanantham, S., Yaashikaa, P.R., George, C.S., 2021. A review on biosynthesis of metal nanoparticles and its environmental applications. Chemosphere. https://doi.org/10.1016/j.chemosphere.2020.128580.

Shafiei, N., Nasrollahzadeh, M., Iravani, S., 2021. Green synthesis of silica and silicon nanoparticles and their biomedical and catalytic applications. Comments Mod. Chem. https://doi.org/10.1080/02603594.2021.1904912.

Sharma, P., Kherb, J., Prakash, J., Kaushal, R., 2021. A novel and facile green synthesis of SiO2 nanoparticles for removal of toxic water pollutants. Appl. Nanosci. https://doi.org/10.1007/s13204-021-01898-1.

Sholehhudin, M., Azizah, R., Sumantri, A., Sham, S.M., Zakaria, Z.A., Latif, M.T., 2021. Analysis of heavy metals (cadmium, chromium, lead, manganese, and zinc) in well water in East Java Province, Indonesia. Malaysian J. Med. Heal. Sci.

Silva, B., Figueiredo, H., Neves, I.C., Tavares, T., 2009. The role of pH on Cr (VI) reduction and removal by arthrobacter viscosus. Int. J. Chem. Biomol. Eng. 43, 59–62.

Sing, K.S.W., 2007. Reporting physisorption data for gas/solid systems with special reference to the determination of surface area and porosity (Provisional). Pure Appl. Chem. https://doi.org/10.1351/pac198254112201.

Song, S.W., Hidajat, K., Kawi, S., 2005. Functionalized SBA-15 materials as carriers for controlled drug delivery: influence of surface properties on matrix-drug interactions. Langmuir. https://doi.org/10.1021/la051167e.

Sorwat, J., Mellage, A., Kappler, A., Byrne, J.M., 2020. Immobilizing magnetite onto quartz sand for chromium remediation. J. Hazard Mater. https://doi.org/10.1016/j.jhazmat.2020.123139.

Sun, Y., Yang, S., Sheng, G., Guo, Z., Wang, X., 2012. The removal of U(VI) from aqueous solution by oxidized multiwalled carbon nanotubes. J. Environ. Radioact. https://doi.org/10.1016/j.jenvrad.2011.10.009.

Toure, A., Wenbiao, D., Keita, Z., Dembele, A., Elzaki, E.E.A., 2019. Drinking water quality and risk for human health in Pelengana commune, Segou, Mali. J. Water Health. https://doi.org/10.2166/wh.2019.004.

Vilardi, G., Ochando-Pulido, J.M., Verdone, N., Stoller, M., Di Palma, L., 2018. On the removal of hexavalent chromium by olive stones coated by iron-based nanoparticles: equilibrium study and chromium recovery. J. Clean. Prod. https://doi.org/10.1016/j.jclepro.2018.04.151.

Vivancos, J., Deshmukh, R., Grégoire, C., Rémus-Borel, W., Belzile, F., Bélanger, R.R., 2016. Identification and characterization of silicon efflux transporters in horsetail (Equisetum arvense). J. Plant Physiol. https://doi.org/10.1016/j.jplph.2016.06.011.

Wahab, R., Ahmad, N., Alam, M., 2020. Silicon nanoparticles: a new and enhanced operational material for nitrophenol sensing. J. Mater. Sci. Mater. Electron. https://doi.org/10.1007/s10854-020-04269-8.

Wan, Z., Cho, D.W., Tsang, D.C.W., Li, M., Sun, T., Verpoort, F., 2019. Concurrent adsorption and micro-electrolysis of Cr(VI) by nanoscale zerovalent iron/biochar/Ca-alginate composite. Environ. Pollut. https://doi.org/10.1016/j.envpol.2019.01.047.

Wang, J., Chen, Z., Chen, W., Li, Y., Wu, Y., Hu, J., Alsaedi, A., Alharbi, N.S., Dong, J., Linghu, W., 2016. Effect of pH, ionic strength, humic substances and temperature on the sorption of Th(IV) onto NKF-6 zeolite. J. Radioanal. Nucl. Chem. https://doi.org/10.1007/s10967-016-4868-4.

Wani, P.A., Wahid, S., Singh, R., Kehinde, A.M., 2018. Antioxidant and chromium reductase assisted chromium (VI) reduction and Cr (III) immobilization by the rhizospheric Bacillus helps in the remediation of Cr (VI) and growth promotion of soybean crop. Rhizosphere. https://doi.org/10.1016/j.rhisph.2018.01.004.

Xu, S., Yu, W., Liu, S., Xu, C., Li, J., Zhang, Y., 2018. Adsorption of hexavalent chromium using banana pseudostem biochar and its mechanism. Sustain. Times. https://doi.org/10.3390/su10114250.

Yadav, N., Garg, V.K., Chhillar, A.K., Rana, J.S., 2021. Detection and remediation of pollutants to maintain ecosustainability employing nanotechnology: a review. Chemosphere. https://doi.org/10.1016/j.chemosphere.2021.130792.

Yao, Y., Mi, N., He, C., Zhang, Y., Yin, L., Li, J., Wang, W., Yang, S., He, H., Li, S., Ni, L., 2020. A novel colloid composited with polyacrylate and nano ferrous sulfide and its efficiency and mechanism of removal of Cr(VI) from Water. J. Hazard Mater. https://doi.org/10.1016/j.jhazmat.2020.123082.

Younis, A.M., Elkady, E.M., Saleh, S.M., 2020. Novel eco-friendly amino-modified nanoparticles for phenol removal from aqueous solution. Environ. Sci. Pollut. Res. https://doi.org/10.1007/s11356-020-09313-y.

Zaumseil, P., 2015. High-resolution characterization of the forbidden Si 200 and Si 222 reflections. J. Appl. Crystallogr. https://doi.org/10.1107/S1600576715004732.

Zhang, H., Peng, L., Chen, A., Shang, C., Lei, M., He, K., Luo, S., Shao, J., Zeng, Q., 2019. Chitosan-stabilized FeS magnetic composites for chromium removal: characterization, performance, mechanism, and stability. Carbohydr. Polym. https://doi.org/10.1016/j.carbpol.2019.03.056.

Zhang, J., Lin, S., Han, M., Su, Q., Xia, L., Hui, Z., 2020. Adsorption properties of magnetic magnetite nanoparticle for coexistent Cr(VI) and Cu(II) in mixed solution. Water 12, 446. https://doi.org/10.3390/w12020446.

Zhou, Z., Liu, J., Zhou, N., Zhang, T., Zeng, H., 2021. Does the "10-Point Water Plan" reduce the intensity of industrial water pollution? Quasi-experimental evidence from China. J. Environ. Manag. https://doi.org/10.1016/j.jenvman.2021.113048.

Zhu, J., Gu, H., Guo, J., Chen, M., Wei, H., Luo, Z., Colorado, H.A., Yerra, N., Ding, D., Ho, T.C., Haldolaarachchige, N., Hopper, J., Young, D.P., Guo, Z., Wei, S., 2014. Mesoporous magnetic carbon nanocomposite fabrics for highly efficient Cr(vi) removal. J. Mater. Chem. https://doi.org/10.1039/c3ta13957c.